Inorganica Chimica Acta 482 (2018) 935–942

Contents lists available at ScienceDirect

Inorganica Chimica Acta

journal homepage: www.elsevier.com/locate/ica

Research paper

π–π interaction leading to an inversion-symmetric complex pair of Λ- and Δ-*bis*[N-2-(R-pyridyl)-2-oxo-1-naphthaldiminato-κ^2*N*,*O*]zinc(II)

Mohammed Enamullah[a,*], Mohammad Ariful Islam[a], Baitul Alif Joy[a], Birger Dittrich[b], Guido J. Reiss[b], Christoph Janiak[b]

[a] Department of Chemistry, Jahangirnagar University, Dhaka 1342, Bangladesh
[b] Institut für Anorganische Chemie und Strukturchemie, Heinrich-Heine-Universität, Universitätsstr. 1, D-40225 Düsseldorf, Germany

ARTICLE INFO

Keywords:
Λ/Δ-configured zinc(II)-Schiff base complexes
Chirality-at-metal centre
Inversion-symmetry
π–π Interactions
DFT/TDDFT

ABSTRACT

The Schiff base ligands N-2-(R-pyridyl)-2-hydroxy-1-naphthaldimine (HL) react with the zinc(II) nitrate or acetate to give the Λ- and Δ-*bis*[N-2-(R-pyridyl)-2-oxo-1-naphthaldiminato-κ^2*N*,*O*]zinc(II), [Zn(L)$_2$] {R = H (**1**), 4/6-CH$_3$ (**2**/**3**)}. EI-mass spectra show the molecular ion peaks at 558 (**1**) and 586 (**2** or **3**). Molecular structure determination for **2**·0.5CH$_2$Cl$_2$ crystal reveals that two molecules of the NˆO-chelate ligands form a tetrahedral N$_2$O$_2$-coordination sphere around the zinc atom, in which one of the pyridyl-N atom is located towards the metal atom at a close contact ([Zn1…N2] = 2.674 Å). Packing analysis explores that one of the Zn-chelate ring metallacycles forms a reciprocal and rather strong π–π interaction (Cg···g = 3.517 Å) with the pyridyl ring of an adjacent molecule and *vice versa*, and results in an inversion-symmetric complex pair with opposite Λ- and Δ-configurations at the metal centre. The packing analysis is further supported by quantitative analysis of intermolecular interactions with the Hirshfeld surface. The optimized structure and excitation state properties by DFT/TDDFT support the solid state molecular structure and electronic spectra in solution, respectively.

1. Introduction

Four-coordinated C_2-symmetrical transition metal(II)-complexes with bidentate NˆO-chelate Schiff-base ligands in tetrahedral to distorted square-planar geometry exhibit induced right(Δ)- and left (Λ)-handed chirality at-metal center [1,2]. Use of chiral enantiopure *R*- or *S*-NˆO-chelate ligands results in the formation of enantiopure chiral-at-metal centered Δ- or Λ-configured complexes in a stereoselective way [3], while achiral chelate ligands give a racemic mixture of Δ/Λ-optical isomers [4]. We have recently given attention to the phenomenon of induced Λ vs. Δ-chirality at-metal centre in four coordinated, non-planar [M(*R*- or *S*-NˆO)$_2$] (M = Co/Ni/Cu/Zn(II) and NˆO = salicylaldiminato/naphthaldiminato Schiff base ligands) with preferred formation of Δ- or Λ-configured diastereomers, as evidenced by X-ray studies, electronic/vibrational circular dichroism (ECD/VCD), H-NMR studies and thermal analyses along with theoretical calculations [5–9]. Our investigations further demonstrate that the induced Λ vs. Δ chirality at-metal centre can be efficiently controlled by the ligand chirality and design, metal ion selection and solute-solvent interactions.

In the context of induced Λ/Δ-chirality at-metal center, we extended the syntheses to zinc/copper(II)-NˆO-chelate complexes using the achiral (R-pyridyl)-Schiff base ligands, N-2-(R-pyridyl)salicylaldimine [10–12] and N-2-(R-pyridyl)-2-hydroxy-1-naphthaldimine (Scheme 1) [13]. X-ray structures demonstrate two deprotonated NˆO-chelate ligands form a tetrahedral N$_2$O$_2$-coordination sphere with Δ/Λ-configured zinc atom in Δ/Λ-*bis*[*N*-2-(pyridyl)salicylaldiminato-κ^2*N*,*O*]zinc (II) [10]. The Δ- and Λ-configured complexes assemble in right (*P*)- and left (*M*)-handed helical chains, resulting spontaneous resolution to racemic conglomerate *via* weak C-H···O hydrogen bonding interactions between the neighbouring molecules. However, an additional weak coordination between the zinc(II) and one or two pyridyl-nitrogen atoms extends the fourfold N$_2$O$_2$-coordination number to 4 + 1 (R = 4-CH$_3$) or 4 + 2 (R = 6-CH$_3$) [11]. The crystals structures feature two weak interactions C-H···π and π···π in five-coordinated or C-H···O and π···π in six-coordinated compounds. In *bis*[N-2-(R-pyridyl)-2-hydroxy-1-naphthaldiminato-κ^2*N*,*O*]copper(II), deprotonated NˆO-chelate ligands form a square-planar N$_2$O$_2$-coordination sphere around the metal atom (Scheme 1) [13]. It is also noted that the pyridyl-Schiff base ligands undergo *in-situ* hydrolysis back to the aldehyde during complexation and/or slow crystallization process and result in the formation of copper(II)-salicylaldehyde complexes [14,15].

The present effort continues to synthesis and characterization of

* Corresponding author.
E-mail address: enamullah@juniv.edu (M. Enamullah).

https://doi.org/10.1016/j.ica.2018.07.028
Received 27 May 2018; Received in revised form 17 July 2018; Accepted 19 July 2018
Available online 20 July 2018
0020-1693/

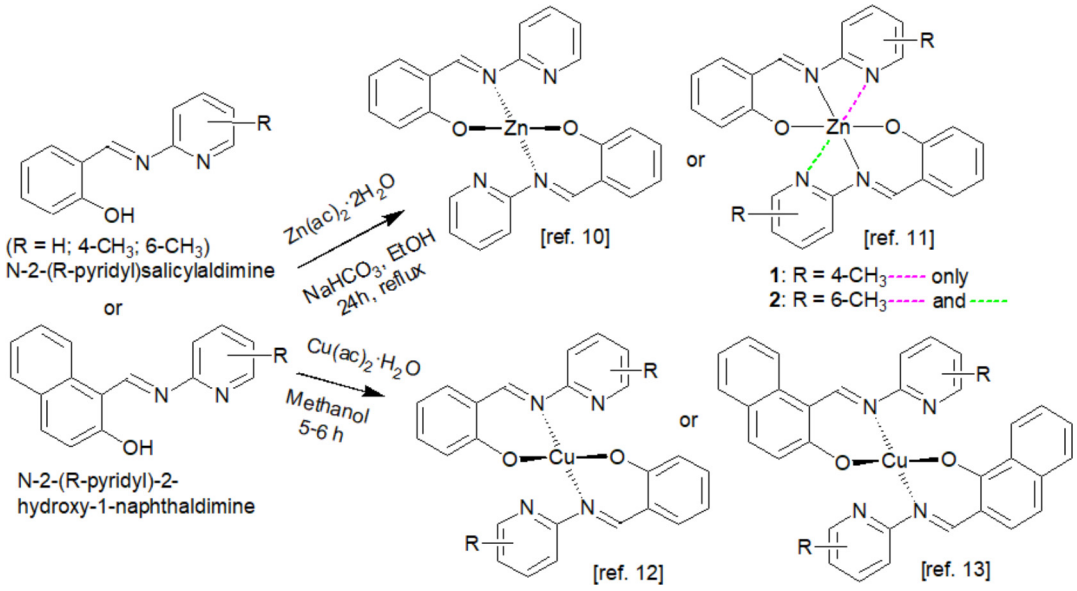

Scheme 1.

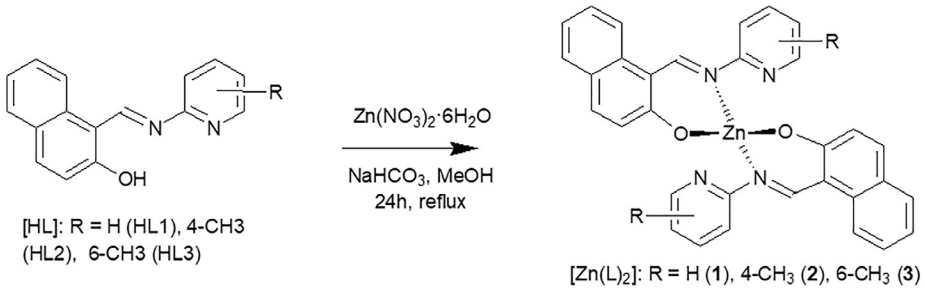

Scheme 2. Synthetic route to complexes Λ- and Δ-*bis*[N-2-(R-pyridyl)-2-oxo-1-naphthaldiminato-κ^2N,O]zinc(II) (**1**–**3**).

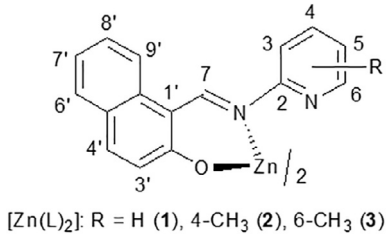

Scheme 3. Protons numbering.

tetrahedral Λ- and Δ-*bis*[N-2-(R-pyridyl)-2-hydroxy-1-naphthaldiminato-κ^2N,*O*]zinc(II) {R = H (**1**); 4-CH_3 (**2**); 6-CH_3 (**3**)} (Scheme 2). Molecular structure of **2**·0.5CH_2Cl_2 explores reciprocal and strong π–π interactions between the zinc(II)-N^O-chelate rings and the pyridyl rings of adjacent molecules, resulting in an inversion-symmetric complex pair of Δ- and Λ-configurations. Quantitative analysis of intermolecular interactions with Hirshfeld surfaces is parallel to the packing analysis. The optimized structure and excitation state properties by DFT/TDDFT are studied to rationalize the molecular structure and electronic spectra, respectively.

2. Experimental

2.1. Materials and measurements

FT-IR spectra were recorded on Nicolet iS10 (Thermo Scientific) spectrometer as KBr discs at ambient temperature. Electronic spectra were obtained with Shimadzu UV 1800 spectrophotometer in $CHCl_3$ at 25 °C. Elemental analyses were performed on a VarioEL from Elementaranalyensysteme. Thermal analysis by Differential Scanning Calorimetry (DSC) was performed on a Shimadzu DSC-60, using at

Table 1
Crystal data and structure refinement for **2**·0.5CH_2Cl_2.

Empirical formula	$C_{34}H_{26}N_4O_2Zn{\cdot}0.5CH_2Cl_2$
M (g mol^{-1})	630.42
Crystal size (mm)	0.18 × 0.09 × 0.08
Temperature (K)	296
θ range (°)	1.70–25.61
h; k; l range	± 17; +26, −27; ± 10
Crystal system	Monoclinic
Space group	$P2_1/c$
a, b, c (Å)	14.3111 (5), 22.284 (2), 9.0464 (10)
β(deg.)	96.781 (6)
V ($Å^3$)	2864.8 (5)
Z	4
D_{calc} [g/cm^{-3}]	1.464
F(0 0 0)/μ (mm^{-1})	1300/0.991
Trans. (max/min)	0.745/0.682
Reflect. collected (R_{int})	91,347 (0.057)
Independent reflections	5352
Obs. reflections [$I > 2\Sigma(I)$]	3457
Data/restraints/parameters	5352/6/398
Largest diff. peak and hole (Δρ/e$Å^{-3}$)	0.52/−0.94
R_1/wR_2 [$I > 2\Sigma(I)$][a]	0.0478/0.1102
R_1/wR_2 (all reflect.)[a]	0.0910/0.1302
Goodness-of-fit on F^2[b]	1.018

[a] $R_1 = [(||F_o| - |F_c||)/|F_o|]$; $wR_2 = [\,[w(F_o^2 - F_c^2)^2]/[w(F_o^2)^2]]^{1/2}$.
[b] Goodness-of-fit = $[\,[w(F_o^2 - F_c^2)^2]/(n-p)]^{1/2}$.

heating range of 298–558 K (before decomposition temperature) and heating rate of 10 K min^{-1}. ^{1}H NMR-spectra were recorded on a Bruker Avance 400 spectrometer operating at 400 MHz (^{1}H) in $CDCl_3$ at 20 °C. Electron impact (EI) mass spectra were obtained on a Finnigan Trace GC Ultra. Isotopic distributions patterns for $^{64/66/68}$Zn(II)-containing ions are clearly visible in the mass spectra. Syntheses of the Schiff bases N-2-(R-pyridyl)-2-hydroxy-1-naphthaldimine {R = H (HL1), 4-CH_3 (HL2) and 6-CH_3 (HL3)} were reported in previous communications [13,16].

2.2. General procedure to synthesise the complexes

Two equivalents of N-2-(pyridyl)-2-hydroxy-1-naphthaldimine (HL1) (0.338 g, 1.36 mmol) dissolved in 10 mL of methanol were added into 5 mL of methanol solution of $Zn(NO_3)_2{\cdot}6H_2O$ (0.203 g, 0.68 mmol). Two equivalents of $NaHCO_3$ (dissolved in 5 mL of methanol) were added into this solution, which was refluxed for 24 h. A bright-yellow precipitate was formed within 2 h of reflux. Reducing the volume of the solvent to *ca.* 50% in *vacuo* led to complete precipitation at room temperature. The precipitate was then filtered off and washed three times with methanol (2 mL in each). Finally, the precipitate was dried in *vacuo* for 12 h at 40 °C to give the bright-yellow product of *bis*[*N*-2-(pyridyl)-2-hydroxy-1-naphthaldiminato-κ^2*N,O*]zinc(II), [Zn(L1)$_2$] (**1**). The same procedure was followed for the syntheses of the compounds *bis*[N-2-(4-methyl-pyridyl)-2-hydroxy-1-naphthaldiminato-κ^2*N,O*]zinc (II), [Zn(L2)$_2$] (**2**) and *bis*[*N*-2-(6-methyl-pyridyl)-2-hydroxy-1-naphthaldiminato-κ^2*N,O*]zinc(II), [Zn(L3)$_2$] (**3**) using the Schiff bases HL2 and HL3, respectively. X-ray quality single crystals for **2**·0.5CH_2Cl_2 were grown by slow diffusion of methanol into a concentrated solution of the sample in dichloromethane at room temperature.

2.2.1. Bis[N-2-(pyridyl)-2-oxo-1-naphthaldiminato-κ^2N,O]zinc(II), [Zn(L1)$_2$] (1)

Yield: 0.280 g (72%). – IR (KBr, cm^{-1}): 3059, 3030w (H-C), 1618, 1604vs (C=N), and 1582, 1564 s (C=C). ^{1}H NMR (400 MHz, $CDCl_3$): δ = 7.09 (d, *J* = 9.2 Hz, 1H, *H3′*), 7.26 (d, *J* = 8.4 Hz, 1H, *H3*), 7.34 (t, *J* = 6.8, 1H, *H5*), 7.54 (t, *J* = 6.0, 1H, *H7*), 7.57 (d, *J* = 6.4 Hz, 1H, *H8′*), 7.71 (dd, *J* = 7.6/1.2 Hz, 1H, *H9′*), 7.73 (dd, *J* = 6.0/3.6 Hz, 1H, *H4*), 7.83 (d, *J* = 9.6, 1H, *H6′*), 8.27 (d, *J* = 8.8, 1H, *H4′*), 8.36 (dd, *J* = 5.0/1.2 Hz, 1H, *H6*) and 10.48 (s, 1H, *H*CN) (see Scheme 3 for proton numbering). – MS (EI): *m/z* = 558 (10) $[M]^+$, 248 (35) $[HL1]^+$ and 93 (1 0 0) $[C_5NH_4(CH_3)]^+$ (M = $C_{32}H_{22}N_4O_2Zn$ and HL1 = $C_{16}H_{12}N_2O$). – $C_{32}H_{22}N_4O_2Zn{\cdot}0.5H_2O$ (568.94): calcd. C, 67.56; H, 4.07; N, 9.85 found C 66.79, H 3.74, N 9.52.

Alternative method

Synthesis of compound **1** using $Zn(CH_3CO_2)_2{\cdot}2H_2O$ was achieved following the same procedure as mentioned above.

Yield: 0.272 g (70%). – IR (KBr, cm^{-1}): 3055, 3033w (H-C), 1619, 1608vs (C=N), and 1586, 1567 s (C=C). – $C_{32}H_{22}N_4O_2Zn{\cdot}1.5H_2O$ (586.96): calcd. C, 65.48; H, 4.29; N, 9.55 found C 65.67, H 3.85, N 10.00.

2.2.2. Bis[N-2-(4-methyl-pyridyl)-2-oxo-1-naphthaldiminato-κ^2N,O]zinc (II), [Zn(L2)$_2$] (2)

Yield: 0.300 g (72%). – IR (KBr, cm^{-1}): 3059, 3036w (H-C), 1616, 1601vs (C=N), and 1583, 1565 s (C=C). ^{1}H NMR (400 MHz, $CDCl_3$): δ = 2.05 (s, 3H, CH_3), 6.82 (d, *J* = 5.0 Hz, 1H, *H3′*), 7.05 (s, 1H, *H3*), 7.08 (d, *J* = 9.2 Hz, 1H, *H5*), 7.31 (t, *J* = 7.1 Hz, 1H, *H7′*), 7.53 (ddd, *J* = 8.4, 8.5/1.2, 1.3 Hz, 1H, *H8′*), 7.69 (d, *J* = 7.8 Hz, 1H, *H9′*), 7.80 (d, *J* = 9.6 Hz, 1H, *H6′*), 8.17 (d, *J* = 5.0 Hz, 1H, *H4′*), 8.23 (d, *J* = 8.5 Hz, 1H, *H6*), and 10.41 (s, 1H, *H*CN) (see Scheme 3 for proton numbering). MS (EI): *m/z* (%) = 586 (15) $[M]^+$, 325 (35) $[M-L2]^+$, 262 (45) $[HL2]^+$ and 93 (1 0 0) $[C_5NH_4(CH3)]^+$ (M = $C_{34}H_{26}N_4O_2Zn$ and HL2 = $C_{17}H_{14}N_2O$). – $C_{34}H_{26}N_4O_2Zn{\cdot}H_2O$ (606.00): calcd. C, 67.39; H, 4.66; N, 9.25 found C 67.98, H 4.29, N 9.08.

2.2.3. Bis[N-2-(6-methyl-pyridyl)-2-oxo-1-naphthaldiminato-κ^2N,O]zinc (II), [Zn(L3)$_2$] (3)

Yield: 0.288 g (70%). – IR (KBr, cm^{-1}): 3055, 3037w (H-C), 1618, 1605vs (C=N), and 1586, 1566 s (C=C). – ^{1}H NMR (400 MHz, $CDCl_3$): δ = 2.28 (s, 3H, CH_3), 6.87 (d, *J* = 7.4 Hz, 1H, *H3′*), 7.09 (d, *J* = 9.2 Hz, 1H, *H3*), 7.14 (d, *J* = 8.1 Hz, 1H, *H5*), 7.32 (ddd, *J* = 7.8, 7.0/0.88, 0.88 Hz, 1H, *H7′*), 7.48 (t, *J* = 7.8 Hz, 1H, *H8′*), 7.55 (dd, *J* = 6.0 Hz, 1H, *H9′*), 7.73 (dd, *J* = 6.0 Hz, 1H, *H4*), 7.80 (dd, *J* = 9.2 Hz, 1H, *H6′*), 8.22 (d, *J* = 8.4 Hz, 1H, *H4′*), and 10.34 (s, 1H, *H*CN) (see Scheme 3 for proton numbering). – MS (EI): *m/z* (%) = 586 (10) $[M]^+$, 325 (30) $[M-L3]^+$, 262 (35) $[HL3]^+$ and 93 (1 0 0) $[C_5NH_4(CH_3)]^+$ (M = $C_{34}H_{26}N_4O_2Zn$ and HL3 = $C_{17}H_{14}N_2O$). – $C_{34}H_{26}N_4O_2Zn{\cdot}1.5H_2O$ (615.01): calcd. C, 66.40; H, 4.75; N, 9.11 found C 66.25, H 4.11, N 8.67.

2.3. Single crystal X-ray diffraction

The solid-state structure of **2**·0.5CH_2Cl_2 was determined by single-crystal X-ray diffraction. Diffraction data were measured using Mo Kα radiation (λ = 0.71073 Å) from an Incoatec microfocus source with mirror optics on a Bruker Apex2 CCD area detector diffractometer with a kappa geometry. Crystals were stable at room temperature and glued onto a glass fibre. Integration was done using the computer program SAINT version 8.37A [17], an empirical absorption correction and scaling were carried out with SADABS [18], which provided the unmerged hkl file for later refinement. The structure was solved using dual space direct methods as implemented in the program SHELXT [19]; full-matrix least-squares refinement on F^2 against all reflections was done using SHELXL 2014/6 [19]. Riding hydrogen atom treatment with U_{iso} constrained to the parent atom was used throughout. For dichloromethane solvent molecule, where the non-hydrogen atoms are situated on special position, suitable constrains ensured that their bond distances remained reasonable. Non-hydrogen atoms were modelled with anisotropic displacement parameters throughout. Visualization model building relied on SHELXLE rev. 799 [20]. Crystal data and details on the structure refinement are given in Table 1.

2.4. Computational method

Computational procedure was carried out with the Gaussian 09 software package [21]. The initial geometry for computation was generated from the X-ray structure of compound **2**. The geometry around the metal atom was kept fixed by constraining the Zn-O and Zn-N bond lengths and the O-Zn-O and *N*-Zn-N bond angles at their respective X-ray values [7]. All the remaining rotatable bonds were included in the geometry optimization by DFT using the functional B3LYP and the basis sets 6-31G(d) and SDD, respectively. Excited state properties by TD-DFT were carried out to rationalize the experimental electronic spectrum in solution. TD-DFT was employed with the combinations of different functionals such as B3LYP, cam-B3LYP and m06 and the basis sets 6-31G(d), SDD and TZVP on the optimized structure by B3LYP/6-31G(d), respectively [7,10,11]. Polarization Continuum Model (PCM) was included using acetonitrile as solvent and 72 excitation states were considered for calculations (Table S4). The spectra were generated using the program SpecDis [22] by applying a Gaussian band shape with a 0.32 eV exponential half-width. For assignments of excited state properties, the molecular orbitals (MOs) calculations were performed using the same level of theory.

3. Results and discussion

The pyridyl Schiff base ligand N-2-(R-pyridyl)-2-hydroxy-1-naphthaldimine (HL) upon deprotonation coordinates to the zinc(II) ion to give Λ- and Δ-*bis*[N-2-(R-pyridyl)-2-oxo-1-naphthaldiminato-κ^2*N,O*] zinc(II), [Zn(L)$_2$] {R = H (**1**) and 4/6-CH_3 (**2/3**)} in the presence of $NaHCO_3$ under reflux for 24 h in methanol (Scheme 2). Vibrational

spectra show strong bands, associated with the coordinated Schiff base ligands, at 1600–1620 cm^{-1} for $\nu C=N$ [5–9]. EI mass spectra show the molecular ion peaks ($[M]^+$) at *m/z* 558 for (**1**) or 586 (**2** or **3**), while the ion peaks for the ligand at *m/z* 248 (HL1) or 262 (HL2 or HL3).

3.1. Electronic spectra and excited state properties

Electronic spectrum of the compound **2** features several bands/shoulders below 500 nm due to intra-ligand (LL) and metal-ligand (ML) electronic transitions in acetonitrile (Fig. S1 in Supp. Info.) [7–11]. The computed spectra by TD-DFT with the combinations of different functionals and the basis sets are almost identical and fit to the experimental one with shifting of the bands positions (Fig. S1 in Supp. Info.). The assignments on computed spectra are vulnerable by the complexity of the system and existences of a large number of transitions at a single excitation state (Table S4 in Supp. Info.) [5–10,13,23]. Thus, some selected and simplified assignments based on orbital and population analyses, pertinent to the experimental spectrum, are listed in Table S1 (in Supp. Info.). A combined ligand-ligand and metal-ligand transitions band is found at *ca.* 380 nm (λ_{max}), which shows the highest molecular orbitals (MOs) contributions of 78% for HOMO-1 to LUMO transitions (Fig. S2 in Supp. Info.).

3.2. ^1H NMR spectra

In the ^1H NMR spectra of the ligands (Fig. 1 for HL2 as example), the methyl protons appear as a singlet at δ 2.42 (HL2) and 2.62 ppm (HL3), which shift to high field upon coordination to the metal ion with δ 2.05 (**2**) and 2.28 ppm (**3**). The phenolic proton (OH) of the free ligand shows a doublet at most down field (*ca.* δ 15.40 ppm, J = 6.4 Hz), which is obviously absent in the coordination compounds. The imine proton shows a doublet at *ca.* δ 9.95 ppm (J = 8.0 Hz) in the free Schiff base ligands, while a singlet at *ca.* 10.40 ppm is found in the coordination compounds. The aromatic H6 proton is found as a doublet of doublet at δ 8.50 ppm (J = 5.0/0.8 Hz) in HL1 and 8.36 ppm (J = 4.8/1.2 Hz) in **1**, while it is a doublet at δ 8.35 ppm (J = 5.6 Hz) in HL2 and 8.23 ppm (J = 8.5 Hz) in **2**. The shift of phenolic-, imine- and H6-protons to relatively low field is due to a strong inductive effect of the adjacent oxygen, π-electrons in the double bond and pyridine nitrogen atom, respectively. Similarly, the methyl protons adjacent to the pyridine nitrogen atom appear at relatively low field by *ca.* 0.20 ppm in HL3 or **3** (i.e., at δ 2.62 or 2.28 ppm) in comparison to those in HL2 or **2** (δ 2.42 or 2.05 ppm). The imine proton shifts to relatively low field by *ca.* 0.50 ppm upon coordination of the ligand to the metal ion, thereby, indicates the formation of Zn-N bond. The spectra further feature several aromatic protons peaks in the range of 6.80–8.30 ppm (see Section 2), which are fully assigned as shown in Fig. 1.

3.3. Hydrolysis of compound *2*

The tetrahedral Zn(II)-Schiff base compounds are labile and undergo rapid hydrolysis back to the free Schiff base ligand in solution. To check the phenomena, we conducted a time dependent ^1H NMR experiment within *ca.* 10 min, 1 h and 20 h of compound dissolution in $CDCl_3$ (containing *ca.* 0.5% H_2O, v/v) (Fig. S3 in Supp. Info.). The results show that the ratio of integration values for C*H*N (or CH_3) group of

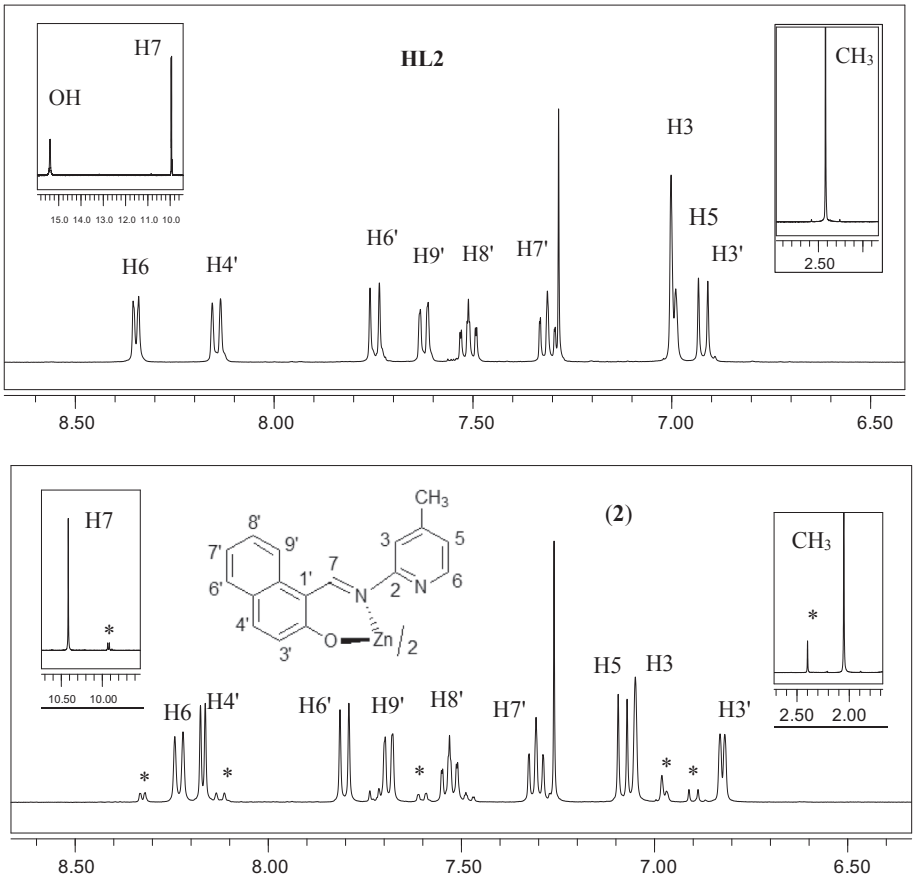

Fig. 1. ^1H NMR spectra of HL2 and **2** in $CDCl_3$ at 20 °C (peaks with asterisks correspond to a little amount of free Schiff base ligand resulting from hydrolysis of **2**, as discussed below).

the ligand (HL2) to the compound (**2**) is *ca.* 0.45/0.55 (HL2/**2**) within 10 min, which changes to 0.56/0.44 within 1 h and to 0.65/0.35 within 20 h of compound dissolution.

3.4. Thermal analyses

The phase transformation from solid to isotropic liquid phase for transition metal(II)-Schiff base complexes is well documented by the Differential Scanning Calorimetry (DSC) analyses [5–8,10–14,24]. The DSC heating curves for compounds **1** and **2** are similar within error and show exothermic peaks at *ca.* 276 (ΔH = −31.9 kJ/mol) and 275 °C (ΔH = −51.0 kJ/mol), respectively (Fig. 2a). The cooling curves show no peaks on the reverse direction, suggesting an irreversible phase transformation or decomposition [5–8,10–14]. The heating curve for **3** in the first cycle shows an exothermic peak at *ca.* 289 °C (ΔH = −58.0 kJ/mole) and the cooling curve shows an endothermic peak at *ca.* 198 °C (ΔH = 36.0 kJ/mol) (Fig. 2b). The heating curve repeated for the second cycle shows a peak at *ca.* 282 °C (ΔH = −49.0 kJ/mole). We interpret this as a higher thermal stability of compound **3**. While compounds **1** and **2** fully decompose around 280 °C, compound **3** melt at about 280 °C with only partial decomposition during first heating. However, there are very small peaks at *ca.* 158 °C (**2**) or 161 °C (**3**), indicate the presence of a small amount of free ligand (HL2 or HL3) in the sample, which is obviously absent in the second heating cycle for **3** due to decomposition.

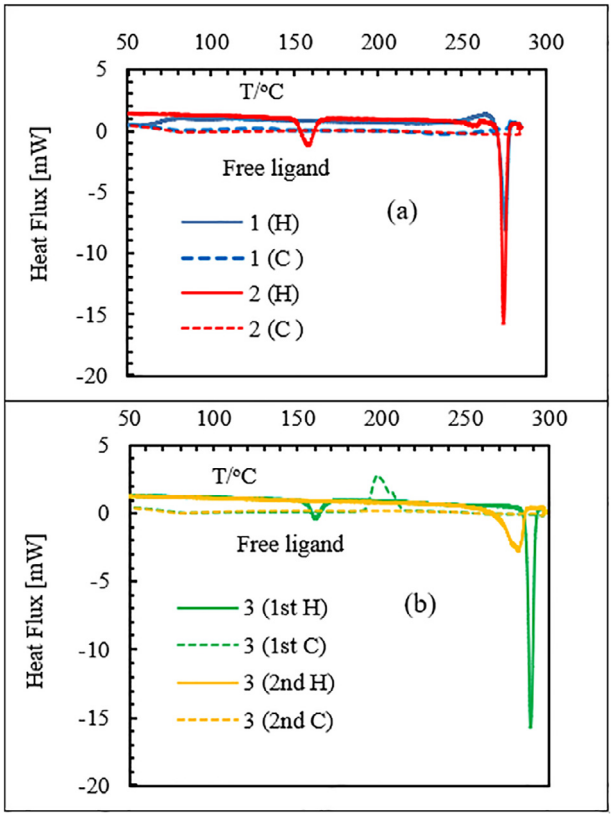

Fig. 2. DSC analyses curves for compounds **1**, **2** (a) and **3** (b) (H = heating, C = cooling).

3.5. X-ray analyses and optimized structures

X-ray molecular structure determination for **2**·0.5CH_2Cl_2 reveals that two molecules of the NˆO-chelate ligands form a tetrahedral N_2O_2-coordination sphere around the zinc atom. There is half a molecule of dichloromethane for each complex molecule and formula unit (**2**·0.5CH_2Cl_2). Fig. 3 shows the molecular structure of **2**. A C_2-symmetry of the metal complex with a twofold axis passing through the metal atom and bisecting the O-Zn-O and *N*-Zn-N angle (along the view direction) is ruled out by the orientation of 4-methyl-pyridy-2yl moiety. The bond lengths and angles in the coordinated ligands (Table 2) are in the expected ranges as for the analogous Zn(II)-NˆO-chelate complexes [7,9,11,16]. It is also noted that one of the pyridyl-N atom is located towards the zinc atom and is in close contact at 2.674 Å [Zn1…N2], which is shorter compared to the related four-coordinated *bis*[N-2-(pyridyl)-2-oxo-1-naphthaldiminato-κ^2N,O]zinc(II) (2.864 Å) [16] and five- or six-coordinated *bis*[N-2-(4- or 6-methylpyridyl)salicylaldiminato-κ^2N,O]zinc(II) (2.750 or 2.714 Å) [11]. In fact, we optimized two possible structures of compound **2** with one pyridyl-N atom (for Δ- and Λ-configurations, Figs. S4A and S4B in Supp. Info.) and both pyridyl-N atoms (Fig. S4C in Supp. Info.) located towards the zinc atom, respectively. The results show that the structures in Figs. S4A and S4B are equi-stable (being isomers), while the structure in Fig. S4C is less stable by *ca.* +3.34 kcal/mol, which are parallel to the crystal structure in Fig. 3.

For quantitative analyses on coordination geometry, along with the optimized structure, the degree of distortion from tetrahedral to square-planar can be calculated from the dihedral angle θ/° (i.e., angle between two planes N1-Zn-O1 and N1′-Zn-O1′) and its normalized function $\tau_{tet\text{-}sq}$ (θ/90°) [5–7,10–13]. The values of θ are 90° (or $\tau_{tet\text{-}sq}$ = 1.0) for tetrahedral and 0° (or $\tau_{tet\text{-}sq}$ = 0) for square-planar geometry (not considering the inherent distortion induced by the chelate ring formation). In **2**·0.5CH_2Cl_2, these values are 88.82° (θ) and 0.99 ($\tau_{tet\text{-}sq}$), close to the optimized structures (i.e., 89.17°/0.99), indicating a tetrahedral geometry around the zinc atom.

The tetrahedral zinc complex **2**·0.5CH_2Cl_2 containing two asymmetric bidentate NˆO-chelate ligands exhibits an induced metal-centered Λ/Δ-chirality [5–7,10–11]. In a centrosymmetric space group as found for the present crystal of **2** ($P2_1/c$) both the Λ- and Δ-configurations must be present (Fig. 4). Indeed, the optimized structures calculated for Δ- and Λ-configured complexes are equally stable (Figs. S4A and S4B in Supp. Info.). However, very little energy difference between the Δ- and Λ-forms (*ca.* 2.74 kcal/mol) is reported in the diastereomeric Λ/Δ-*bis*[{(*R*)-N-(Ar)ethyl-2-oxo-1-naphthaldiminato-κ^2N,O}]zinc(II) [7].

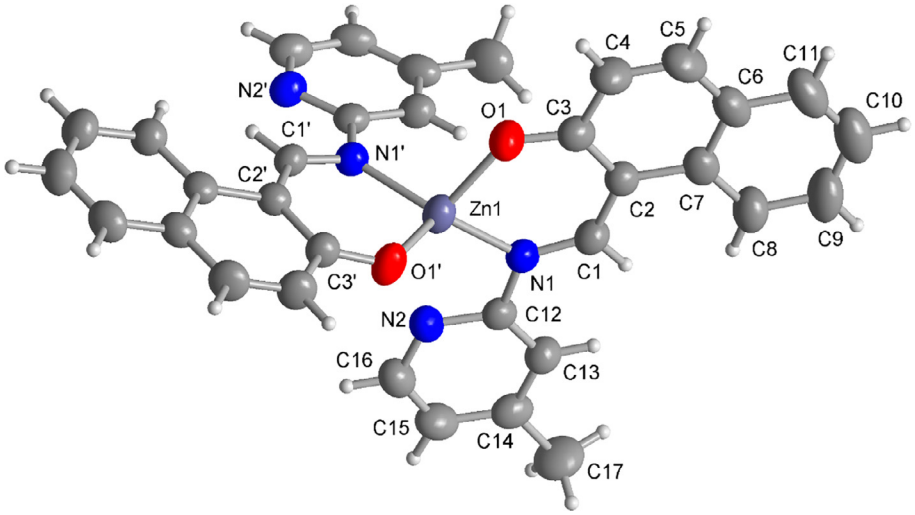

Fig. 3. Molecular structure of compound **2** showing the Δ-configuration. Note that the prime at the atom labels of the second ligand does not imply a symmetry correlation to the first ligand.

Table 2
Selected bond lengths (Å) and angles (°) in compound **2**·0.5CH_2Cl_2.[#]

Zn1-O1/Zn1-O1′	1.982(3)/1.923(2)
Zn1-N1/Zn1-N1′	1.983(3)/1.982(3)
Zn1-N2	2.674(3)
O1-Zn1-N1/O1′-Zn1-N1′	89.89(11), 96.04(10)
O1-Zn1-N1′/N1-Zn1-O1′	107.40(11), 124.45(11)
O1-Zn1-O1′	107.49(12)
N1-Zn1-N1′	129.06(11)

[#] Values are same for both the Δ- and Λ-configured complexes.

3.6. Packing analyses

Packing analyses show that one of the Zn-chelate ring metallacycles of the complex forms a reciprocal and rather strong π–π interaction (Cg…Cg = 3.517 Å, interplanar angle alpha = 1.1°, slip angle β, γ ≈ 15.5°, slippage 0.96 Å) with the pyridyl fragment of an adjacent complex and *vice versa* in the packing of the structure (Table S2 in Supp. Info., Fig. 4). Significant π-stackings show rather short centroid-centroid contacts (< 3.8 Å), near parallel ring planes (alpha < 10° to ~0° or even exactly 0° by symmetry), small slip angles (β, γ < 25°) and vertical displacements (slippage < 1.5 Å) which translate into a sizable overlap of the aryl-plane areas (Scheme S1 in Supp. Info.) [25,26]. *Masui* had suggested an active electron delocalization within a metal-*N*-heterocyclic chelate ring in such a way that it could exhibit some degree of "metalloaromaticity" [27,28]. Thereby the strong π–π interaction (Cg···Cg) forms an inversion-symmetric complex pair of Λ- and Δ-configured complexes (Fig. 4). There are three weak hydrogen bond interactions at distances of 2.56 Å ($d_{H\cdots A}$) from O1′ to pyridyl-H on C13, 2.60 Å from pyridyl-N2′ to pyridyl-H on C15′ and 2.22 Å from pyridyl-N2′ to imino-H on C1′ (Table S3 in Supp. Info.).

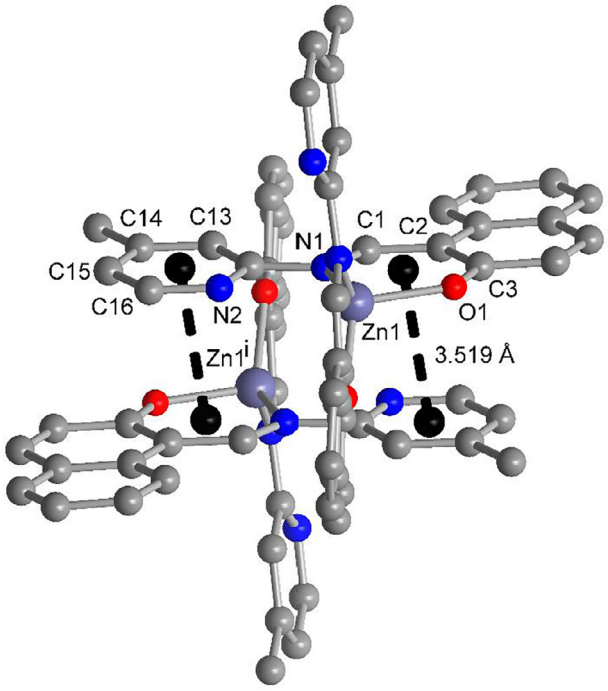

Fig. 4. Reciprocal short π–π interaction between the Zn-N^O-chelate rings and a pyridyl rings in an inversion-symmetric Λ- and Δ-configured "dimer". Symmetry transformation i = 1 − x, 1 − y, 1 − z.

3.7. Hirshfeld surfaces analyses

The packing analysis in **2**·0.5CH_2Cl_2 is further supported by a

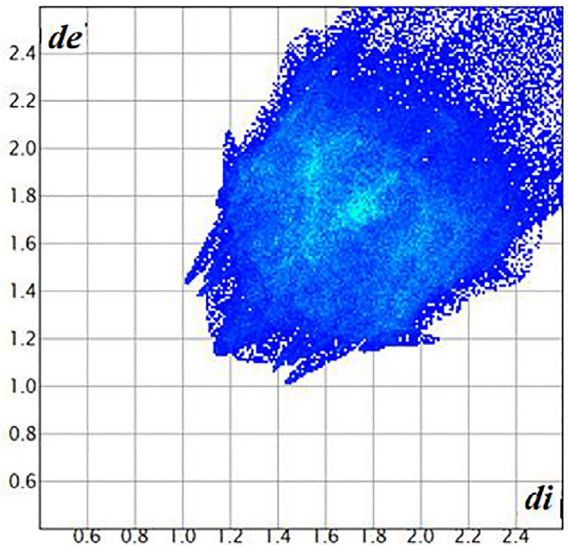

Fig. 5. 2D fingerprint plot of **2**·0.5CH_2Cl_2 with the characteristic features due to the C···C, O···H, N···H, C···H and H···H contacts. d_i and d_e are the distances from the surface to the nearest atom interior and exterior to the surface, respectively. Breakdown of the plot into the corresponding contributions from C···C, O···H, N···H, C···H and H···H close intermolecular contacts is shown Fig. S5 in Supp. Info.

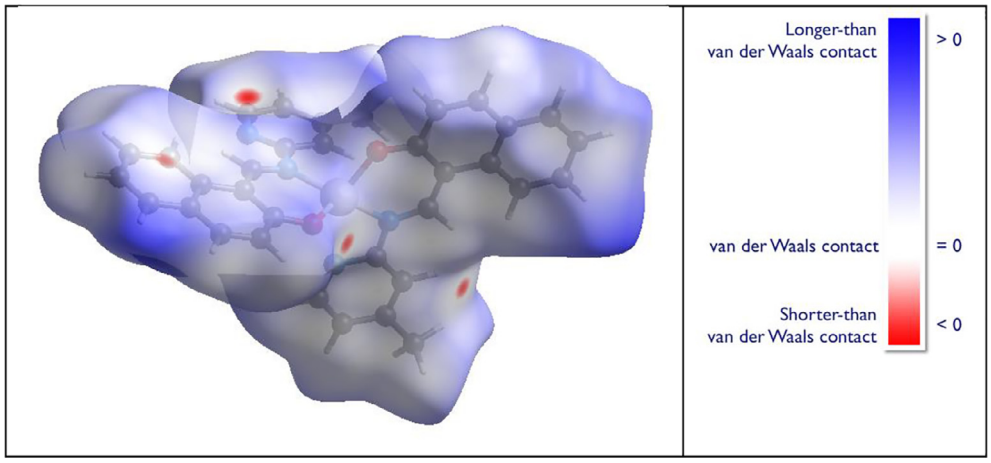

Fig. 6. Hirshfeld surface of compound **2**·0.5CH_2Cl_2 mapped with the d_{norm} property [30c] (red represents the closest contacts, while blue the most distant contacts). Breakdown of the d_{norm} property is shown Fig. S5 in Supp. Info. (For interpretation of the references to colour in this figure legend, the reader is referred to the web version of this article.)

quantitative analysis of intermolecular interactions with Hirshfeld surfaces using the program CrystalExplorer [29] following the methodology outlined in the references [30]. The 2D fingerprint plot (Fig. 5) is an overlay of different contributions arising from close intermolecular contacts. The relative contributions to the Hirshfeld surface area due to these contacts are C···C (i.e. π···π) 5.2%, C···H (i.e. C–H···π) 31.9%, O···H 7.6%, N···H 5.9% and H···H 47.9% (Fig. S5 in Supp. Info.). The plot exhibits the O···H and N···H contacts as two sharp features pointing to the lower left of the plot, respectively. The upper one corresponds to the H-bond donor and lower one to the acceptor [30b]. Hirshfeld surface mapped with d_{norm} property [30c] displays clearly some closest contacts (red circles on the d_{norm} surface in Fig. 6) for strong π–π interactions and some hydrogen bonds interactions as discussed above.

4. Conclusions

Structural analysis for Λ- and Δ-*bis*[N-2-(4-methyl-pyridyl)-2-oxo-1-naphthaldiminato-κ^2N,O]zinc(II) (**2**·0.5CH_2Cl_2) reveals that two NˆO-chelate ligands organize a tetrahedral N_2O_2-coordination sphere around the zinc atom with one of the pyridyl-N atom directed towards the metal atom. Packing analysis explores that one of the Zn-chelate ring metallacycle forms a reciprocal and strong π–π interaction with the pyridyl ring of an adjacent molecule and *vice versa*, results in an inversion-symmetric pair of Δ- and Λ-configured complexes. The packing analysis is further supported by quantitative analysis of intermolecular interactions with Hirshfeld surface analysis. The optimized structure and excitation state properties by DFT/TDDFT correspond well to the solid state molecular structure and electronic spectra in solution, respectively.

Acknowledgement

We acknowledge the Wazed Miah Science Research Centre (WMSRC) at Jahangirnagar University, Dhaka, Bangladesh for obtaining the elemental and ^{1}H NMR data.

Appendix A. Supplementary data

Supplementary data associated with this article can be found, in the online version, at https://doi.org/10.1016/j.ica.2018.07.028.

References

[1] (a) A. von Zelewsky, Stereochemistry of Coordination Compounds, John Wiley & Sons, Chichester, 1996, p. 69;
(b) H. Amouri, M. Gruselle, Chirality in Transition Metal Chemistry: Molecules, Supramolecular Assemblies and Materials, John Wiley & Sons, Chichester, 2008, p. 40;
(c) K.A. Jensen, Inorg. Chem. 9 (1970) 1.
[2] (a) C. Evans, D. Luneau, J. Chem. Soc. Dalton Trans. (2002) 83;
(b) H. Sakiyama, H. Okawa, N. Matsumoto, S. Kida, Bull. Chem. Soc. Jpn. 64 (1991) 2644;
(c) H. Sakiyama, H. Okawa, N. Matsumoto, S. Kida, J. Chem. Soc. Dalton Trans. (1990) 2935;
(d) H. Ōkawa, M. Nakamura, S. Kida, Inorg. Chim. Acta 120 (1986) 185;
(e) T. Akitsu, Y. Einaga, Polyhedron, 24, pp. 2005–2933; ibid, 24 (2005) 1869.
(f) T. Akitsu, Y. Einaga, Acta Crystallogr. C 60 (2004) m640
[3] (a) E.V. Anokhina, A.J. Jacobson, J. Am. Chem. Soc. 126 (2004) 3044;
(b) S.P. Anthony, T.P. Radhakrishnan, Chem. Commun. (2004) 1058;
(c) J. Heo, Y.-M. Jeon, C.A. Mirkin, J. Am. Chem. Soc. 129 (2007) 7712;
(d) L. Jiang, X.-L. Feng, C.-Y. Su, X.-M. Chen, T.-B. Lu, Inorg. Chem. 46 (2007) 2637;
(e) L. Ohrstrom, K. Larsson, S. Borg, S.T. Norberg, Chem. Eur. J. 7 (2001) 4805;
(f) A. Roth, D. Koth, M. Gottschaldt, W. Plass, CrystGrowthDes. 6 (2006) 2655.
[4] (a) C.S. Isfort, T. Kreickmann, T. Pape, R. Froehlich, F.E. Hahn, Chem. Eur. J. 13 (2007) 2344;
(b) H.-J. Kim, E. Lee, H.-S. Park, M. Lee, J. Am. Chem. Soc. 129 (2007) 10994;
(c) R. Wang, Y. Zhou, Y. Sun, D. Yuan, L. Han, B. Lou, B. Wu, M. Hong, CrystGrowthDes. 5 (2005) 25;
(d) S.-T. Wu, Y.-R. Wu, Q.-Q. Kang, H. Zhang, L.-S. Long, Z. Zheng, R.-B. Huang, L.-S. Zheng, Angew. Chem. Int. Ed. 46 (2007) 8475;
(e) Y. Zhang, J. Li, J. Chen, Q. Su, W. Deng, M. Nishiura, T. Imamoto, X. Wu, Q. Wang, Inorg. Chem. 39 (2000) 2330.
[5] M. Enamullah, A.K.M. Royhan Uddin, G. Pescitelli, R. Berardozzi, G. Makhloufi, V. Vasylyeva, A.-C. Chamayou, C. Janiak, Dalton Trans. 43 (2014) 3313.
[6] M. Enamullah, M.A. Quddus, M.R. Hasan, G. Pescitelli, R. Berardozzi, G. Makhloufi, V. Vasylyeva, C. Janiak, Dalton Trans. 45 (2016) 667.
[7] M. Enamullah, G. Makhloufi, M. Refat, B.A. Joy, M.A. Islam, D. Padula, H. Hunter, G. Pescitelli, C. Janiak, Inorg. Chem. 55 (2016) 6449.
[8] M. Enamullah, M.A. Quddus, M.R. Hasan, G. Pescitelli, R. Berardozzi, G.J. Reiß, C. Janiak, Eur. J. Inorg. Chem. (2015) 2758.
[9] M. Enamullah, V. Vasylyeva, C. Janiak, Inorg. Chim. Acta 408 (2013) 109.
[10] M. Enamullah, V. Vasylyeva, M.A. Quddus, M.K. Islam, S.-P. Höfert, C. Janiak, CrystEngComm. (2018), https://doi.org/10.1039/C8CE00839F.
[11] M. Enamullah, M.A. Quddus, M.A. Halim, M.K. Islam, V. Vasylyeva, C. Janiak, Inorg. Chim. Acta 427 (2015) 103.
[12] M. Enamullah, M.A. Quddus, M.M. Rahman, T.E. Burrow, J. Mol. Struct. 1130 (2017) 765.
[13] M. Enamullah, M.A. Islam, B.A. Joy, G.J. Reiss, Inorg. Chim. Acta 453 (2016) 202.
[14] M. Enamullah, A.-C. Chamayou, K.S. Banu, A.-Ch. Kautz, C. Janiak, Inorg. Chim. Acta 464 (2017) 186.
[15] (a) K. Sarmah, G. Pandit, A.B. Das, B. Sarma, S. Pratihar, CrystGrowthDes. 17 (2017) 368;
(b) G.Q. Zhang, G.Q. Yang, J.S. Ma, J. Chem. Res. (2006) 19.
[16] T. Hökelek, Z. Kılıc, M. Isıklan, M. Toy, J. Mol. Struct. 523 (2000) 61.
[17] Bruker APEX2 (Version 2014.11) and SAINT (Version 8.37A). Bruker AXS 2013 Inc Madison, Wisconsin, USA.
[18] L. Krause, R. Herbst-Irmer, G.M. Sheldrick, D. Stalk, J. Appl. Cryst. 48 (2015) 3.
[19] G.M. Sheldrick, Acta Cryst. A71 (2015) 3.
[20] C.B. Huebschle, G.M. Sheldrick, B. Dittrich, J. Appl. Cryst. 44 (2011) 1281.
[21] Gaussian 09, Revision D.01, M.J. Frisch, G.W. Trucks, H.B. Schlegel, G.E. Scuseria, M.A. Robb, J.R. Cheeseman, G. Scalmani, V. Barone, B. Mennucci, G.A. Petersson, H. Nakatsuji, M. Caricato, X. Li, H.P. Hratchian, A.F. Izmaylov, J. Bloino, G. Zheng, J.L. Sonnenberg, M. Hada, M. Ehara, K. Toyota, R. Fukuda, J. Hasegawa, M. Ishida, T. Nakajima, Y. Honda, O. Kitao, H. Nakai, T. Vreven, J.A. Montgomery, Jr., J.E. Peralta, F. Ogliaro, M. Bearpark, J.J. Heyd, E. Brothers, K.N. Kudin, V.N. Staroverov, R. Kobayashi, J. Normand, K. Raghavachari, A. Rendell, J.C. Burant, S. S. Iyengar, J. Tomasi, M. Cossi, N. Rega, J.M. Millam, M. Klene, J.E. Knox, J.B. Cross, V. Bakken, C. Adamo, J. Jaramillo, R. Gomperts, R.E. Stratmann, O. Yazyev,

A.J. Austin, R. Cammi, C. Pomelli, J.W. Ochterski, R.L. Martin, K. Morokuma, V.G. Zakrzewski, G.A. Voth, P. Salvador, J.J. Dannenberg, S. Dapprich, A.D. Daniels, Ö. Farkas, J.B. Foresman, J. V. Ortiz, J. Cioslowski, D.J. Fox, Gaussian, Inc., Wallingford CT, 2009.

[22] T. Bruhn, A. Schaumlöffel, Y. Hemberger, G. Bringmann, Chirality 25 (2013) 243.

[23] A. Ipatov, F. Cordova, L.J. Doriol, M.E. Casida, J. Mol. Struct. (THEOCHEM) 914 (2009) 60.

[24] (a) S. Yamada, Coord. Chem. Rev. 190–192 (1999) 537;
(b) T. Akitsu, Y. Einaga, Polyhedron 25 (2006) 1089;
(c) T. Akitsu, Polyhedron 26 (2007) 2527.

[25] (a) X.-J. Yang, F. Drepper, B. Wu, W.-H. Sun, W. Haehnel, C. Janiak, Dalton Trans., (2005) 256 and Supplementary Material therein; (b) C. Janiak, J. Chem. Soc. Dalton Trans. (2000) 3885.

[26] (a) V. Lozan, P.-G. Lassahn, C. Zhang, B. Wu, C. Janiak, G. Rheinwald, H. Lang, π-Interactions between pyridyl-type ligands for comparison, Z. Naturforsch. B. 58 (2003) 1152;
(b) C. Zhang, C. Janiak, Z. Anorg, Allg. Chem. 627 (2001) 1972;
(c) C. Zhang, C. Janiak, J. Chem. Crystallogr. 31 (2001) 29;
(d) H.-P. Wu, C. Janiak, G. Rheinwald, H. Lang, J. Chem. Soc. Dalton Trans. (1999) 183;
(e) C. Janiak, L. Uehlin, H.-P. Wu, P. Klüfers, H. Piotrowski, T.G. Scharmann, J. Chem. Soc. Dalton Trans. (1999) 3121;
(f) H.-P. Wu, C. Janiak, L. Uehlin, P. Klüfers, P. Mayer, Chem. Commun. (1998) 2637.

[27] H. Masui, Coord. Chem. Rev. 219–221 (2001) 957.

[28] (a) A. Castiñeiras, A.G. Sicilia-Zafra, J.M. Gonzáles-Pérez, D. Choquesillo-Lazarte, J. Niclós-Gutiérrez, Inorg. Chem. 41 (2002) 6956;
(b) E. Craven, C. Zhang, C. Janiak, G. Rheinwald, H. Lang, Z. Anorg, Allg. Chem. 629 (2003) 2282;
(c) H.H. Monfared, Z. Kalantari, M.-A. Kamyabi, C. Janiak, Z. Anorg, Allg. Chem. 633 (2007) 1945.

[29] (a) CrystalExplorer17, Version 17.5; (b) M.J. Turner, J.J. McKinnon, S.K. Wolff, D.J. Grimwood, P.R. Spackman, D. Jayatilaka, M.A. Spackman, © 2005-217 University of Western Australia, 2017. http://hirshfeldsurface.net.

[30] (a) J.J. McKinnon, M.A. Spackman, A.S. Mitchell, Acta Cryst. B60 (2004) 627;
(b) M.A. Spackman, J.J. McKinnon, CrystEngComm. 4 (2002) 378;
(c) J.J. McKinnon, D. Jayatilaka, M.A. Spackman, Chem. Commun. (2007) 3814.